PHYSICAL REVIEW A VOLUME 45, NUMBER 6 15 MARCH 1992

Investigation of the homogeneous-shear nonequilibrium-molecular-dynamics method

Steven Y. Liem, David Brown, and Julian H. R. Clarke*
Department of Chemistry, University of Manchester Institute of Science and Technology, Manchester, M60 1QD, United Kingdom
(Received 2 May 1991)

The homogeneous-shear (HS) technique has been used extensively to study shear flow, but it uses artificial methods to remove the viscous heat generated. In reality the viscous heat is removed from the system by conduction out through the boundaries. This inevitably leads to characteristic gradients in temperature, density, and shear rate. While at low shear rates these effects may be neglected, and the use of HS justified, at high shear rates they certainly cannot, and doubts remain as to the validity of HS in this regime. In this study we make careful comparisons between HS and a more-realistic sliding-boundary method. HS gives very similar results when conditions corresponding to different regions within the sliding system are used. The use of HS simulations at shear rates where energy is generated at a rate faster than can be realistically removed by any natural process is called into question.

PACS number(s): 47.50.+d, 47.25.Ei, 44.90.+c, 66.20.+d

I. INTRODUCTION

During the last two decades there have been a number of methods devised to compute fluid shear viscosities by nonequilibrium molecular dynamics (NEMD), e.g., Refs. [1–8]. Of these, the homogeneous-shear (HS) method has proved to be the most popular. In this method planar Couette flow is imparted on the sample using Lees-Edwards [2] periodic-boundary conditions in order to measure the average stress response. The shear viscosity is then computed using the expression

$$\eta(\dot\gamma)=\frac{-\langle P_{\alpha\beta}\rangle}{\dot\gamma}\ , \tag{1}$$

where $\dot\gamma=\partial u_\alpha/\partial\beta$ is the shear rate, u_α is the α component of the local flow velocity vector $\mathbf{u}$, and $P_{\alpha\beta}$ is the appropriate off-diagonal component of the pressure tensor. The problem with this method is that it is necessary to use large values of $\dot\gamma$ for the small samples employed in simulations in order to achieve an acceptable error ($<10\%$) in $\langle P_{\alpha\beta}\rangle$. In most cases these shear rates are orders of magnitude larger than those employed in even the most extreme experimental studies, and it is necessary to control the temperature artificially in order to achieve steady state. In the HS method, for instance, this can be done by *ad hoc* rescaling [1], by loose coupling [9], by utilizing the Nosé-Hoover thermostat [10,11], or by using the method of Gaussian least constraint [12]. The latter two methods both incorporate the temperature control into the equations of motion. Tests have shown [8], however, that the results are insensitive to the type of thermostat used. The problem with any of these methods is that it is uncertain to what extent the necessary interference with the Newtonian equations of motion affects the structural dynamics of the fluid. For this reason the HS method has been criticized and the physical relevance of the results of such calculations, particularly in the very-high-shear-rate regime where considerable amounts of thermal energy have to be removed, has remained in doubt.

A more realistic simulation of a laboratory shear flow can be achieved by using sliding boundaries (SB). These were first employed by Ashurst and Hoover [1] to investigate the shear viscosity of a dense fluid. In this case the fluid region is bounded above and below by walls which translate in opposite directions to produce a shear flow. In this method the trajectories of the fluid are generated from unmodified Newtonian equations of motion and so evolve naturally with the heat being removed by conduction out through the walls.

As a method for extrapolating the limiting low-shear-rate viscosity, the SB method has been largely discarded due to the boundary effects, minimization of which involves using a relatively large system size. In contrast, it has been shown [13] that for the simple atomic system used here the HS method produces results that are relatively insensitive to system size above $N\approx200$. In this article our primary concern is not the relative merits of these two methods for the calculation of the limiting zero-shear-rate viscosity. There is no doubt in our minds that in this case HS is the technique to use. Whether this is to be preferred over the Green-Kubo or other equilibrium techniques is another question entirely, and one which will not be addressed here.

Our main inquiry here is, given that in the SB case temperature, density, and shear rate vary across the system, how well does a homogeneous system with input parameters $(\rho,T,\dot\gamma)$, taken from the averages at a particular point of the SB system, reproduce the pressure tensor measured in the SB case? It has long been established [14] that above a certain shear rate, homogeneous thermostated systems display normal pressure differences and nonequipartition of the kinetic energy between the x, y, and z directions. Whether these are the result of a real effect (normal pressure differences certainly occur in, e.g., polymeric systems [15]) or originate from the artificial

way in which the heat is removed has not been established. It has already been shown that the "string phases" [16] that occur at very high shear rates can be eliminated by switching to a profile-unbiased thermostat [17]. It was suggested [18] some time ago that a close comparison be made between HS and a large-scale boundary-driven shear simulation. In this paper we present the results of such a comparison.

Our original intention was to probe into the shear-rate regime where nonequipartition and normal pressure differences start to occur. For reasons which we shall discuss later, this proved very difficult to do using the SB method to be described here. This in itself has some important implications regarding HS simulations at high shear rates. The comparison we report is at about the highest possible shear rate for which our SB system is stable, the rationale here being that if differences do exist they are most likely to occur at the highest possible shear rate.

In the SB method we have used very large samples (>40 000 particles) to minimize the boundary effect. Only the temperature of the boundary particles is controlled by using the *ad hoc* momenta-rescaling scheme. This provides a mechanism for removal of heat from the fluid by thermal conduction and leads to the establishment of characteristic temperature and density profiles in the fluid.

In Sec. II we will first describe in detail the SB and HS model systems used to perform the simulations. The results and discussion will be presented in Sec. III and a brief conclusion in Sec. IV.

II. DETAILS OF MODELS AND SIMULATIONS

A. Interaction potential

In this particular study we have used a model atomic fluid. The shifted and truncated Lennard-Jones 12-6 potential, often termed the Weeks-Chandler-Anderson (WCA) potential, is used to describe the interaction between particles,

$$\phi(r)=\begin{cases}4\varepsilon\left[\left(\frac{\sigma}{r}\right)^{12}-\left(\frac{\sigma}{r}\right)^{6}\right]+\varepsilon & \text{for } r\le r_0 \quad (2a)\\ 0, & \text{for } r>r_0 \quad (2b)\end{cases}$$

where $r_0=2^{1/6}\sigma$ is the distance at which the potential is a minimum in the full Lennard-Jones 12-6 potential, σ is the "collision diameter," and ε is the well depth. All properties will be quoted in units reduced by ε, σ, and the mass of a particle, m.

B. Sliding-boundary model

In the SB model the system is composed of an orthorhombic cell which is split into three regions in the y direction; the top and bottom boundary layers with the bulk fluid, containing N_{fluid} particles in a region of dimensions $L_x\times L_y\times L_z$, sandwiched between them (see Fig. 1). Each boundary contains N_{wall} particles arranged in just three hexagonal-close-packed layers. This was considered to provide an adequate barrier to fluid-particle penetration and to be sufficiently deep in view of the short interaction range of the WCA potential. Periodic-boundary conditions are imposed only in the x and z directions to give a laminar model.

For simplicity, the particles in the boundary are exactly the same as those in the fluid; the same WCA potential acts between all the particles in the system. The boundary particles, however, are each subjected to an additional harmonic potential with respect to the hexagonal lattice points $\mathbf{r}_{\text{eq}}$,

$$\phi(|\mathbf{r}(t)-\mathbf{r}_{\text{eq}}|)=\tfrac{1}{2}k_w(|\mathbf{r}(t)-\mathbf{r}_{\text{eq}}|)^2\ , \quad (3)$$

where $\mathbf{r}(t)$ is the position of a boundary particle at time t. For particles in the walls, coordinates and velocities are specified with respect to a set of axes embedded in each boundary. Their positions with respect to the fixed set of axes at the center of the fluid region are obtained by the appropriate transformations. The rigidity of the wall is determined by the force constant k_w and the value used $(72\varepsilon/2^{1/3}\sigma^2)$ is obtained by putting $r=r_0$ in the second derivative of the interaction potential [Eq. (2a)]. The purpose of the harmonic potential is to maintain the lattice structure of the boundary while simultaneously providing freedom for the boundary particles to act as a sink for the viscous heat.

Shear flow is induced in the fluid system by translating the origin of axes for the walls, and hence the wall particles, along the x axis a distance Δx at each time step,

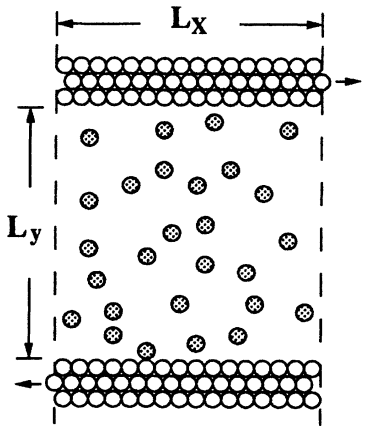

FIG. 1. A 2D schematic representation of our three-dimensional sliding-boundary system (the z dimension is perpendicularly out of the plane of the paper). The shaded and open circles represent the fluid and boundary particles, respectively. Note that the actual ratio of fluid to boundary particles is quite different than is implied by the diagram. The arrows indicate the direction in which the walls slide in order to impose a shear field on the fluid. The dashed lines indicate the position of the periodic boundaries in the x direction. Periodic boundaries are also used in the z direction.

such that

$$\Delta x = \pm \tfrac{1}{2} \dot{\gamma}_a L_y \Delta t \ , \tag{4}$$

where $L_y + \sigma$ is the distance between the two boundaries, as defined by the anchoring lattice points of the layers nearest the fluid; Δt is the time step used in the simulation; and $\dot{\gamma}_a$ is the applied shear rate. The term Δx is positive for the top boundary and negative for the bottom boundary. As a result of this shearing action, heat is constantly generated in the fluid. This heat must be removed from the system if a steady state is to be reached. This is achieved by using the *ad hoc* momenta-rescaling scheme [1]. For this particular system only the boundary particles are thermostatted and the two walls are treated independently. The top and bottom boundary temperatures are evaluated using

$$T_w = \frac{1}{3N_{\text{wall}} k_B} \sum_{i=1}^{N_{\text{wall}}} m_i \mathbf{v}_i^2 \ , \tag{5}$$

where $\mathbf{v}_i$ is the particle velocity with respect to the moving set of axes embedded in the appropriate wall. Two independent scaling factors are then calculated from these temperatures and used to rescale the momenta of the corresponding wall particles at each time step.

In the SB model we calculate the normal and tangential y components of the pressure tensor, P_{yy}, P_{xy}, and P_{zy}, from the forces on the wall particles:

$$P_{\alpha y} = \sum_{i=1}^{N_{\text{wall}}} \sum_{j=1}^{N_{\text{fluid}}} F_{ij}^{\alpha} / A \ , \tag{6}$$

where α represents x, y, or z; A $(=L_x \times L_z)$ is the area of the fluid-boundary interface; and F_{ij}^{α} is the α component of force on particle i due to j. We have also used the virial-theorem expression for the pressure tensor

$$\mathbf{P} = \frac{1}{V} \left\langle \sum_{i=1}^{N_{\text{fluid}}} m_i [\mathbf{v}_i - \mathbf{u}(\mathbf{r}_i)][\mathbf{v}_i - \mathbf{u}(\mathbf{r}_i)] + \sum_{i=1}^{N_{\text{fluid}}} \sum_{j>i}^{N_{\text{fluid}}} \mathbf{r}_{ij} \mathbf{F}_{ij} \right\rangle \ , \tag{7}$$

where V is the volume of the fluid system, $\mathbf{u}(\mathbf{r}_i)$ is the local streaming velocity at position $\mathbf{r}_i$, and $\mathbf{v}_i$ is the total velocity of particle i. In this case two problems arise due to the presence of the physical walls. Without going into great detail, the first arises from the relatively ill-defined dimension of the fluid cell in the y direction; this, of course, affects in turn the value for the volume to use in Eq. (7). We have found that the walls are on average pushed back slightly by the fluid and we discuss later how an average volume is calculated. The second problem arises in the definition of the local streaming velocity, which in the case of boundary driven shear cannot be assumed to take any simple functional form. This problem only affects the kinetic components and is related to the calculation of a local temperature which is discussed below.

For the geometry of the system described, we expect there to be a dependence of the properties only on the perpendicular distance from the walls, i.e., in the y direction. We have, therefore, calculated the variation in the density, flow velocity, and temperature as a function of y by splitting the region between the walls into a number of slabs N_{slab} or width Δy. If we define the function $H_n(y_i)$ such that

$$H_n(y_i) = 1 \quad \text{if } (n-1)\Delta y < y_i - y_0 < n \Delta y \ , \tag{8}$$

where y_0 is the coordinate of some arbitrary point below the lower wall; otherwise,

$$H_n(y_i) = 0 \ . \tag{9}$$

Then the instantaneous reduced number density of a slab $\rho^*(y_n,t)$ can be determined by

$$\rho^*(y_n,t) = \frac{\sigma^3}{A \Delta y} \sum_{i=1}^{N_{\text{fluid}}} H_n(y_i(t)) \ . \tag{10}$$

Here y_n is the coordinate of the midpoint of the nth slab. Similarly, the instantaneous slab velocity $\mathbf{u}(y_n,t)$ is given by

$$\mathbf{u}(y_n,t) = \sum_{i=1}^{N_{\text{fluid}}} H_n(y_i(t)) \mathbf{v}_i(t) \ . \tag{11}$$

Using Eq. (11), we attempted to calculate the slab temperatures in the x, y, and z directions from

$$T_{\alpha}(y_n,t) = \frac{\sum_{i=1}^{N_{\text{fluid}}} H_n(y_i(t)) m_i [v_{\alpha_i}(t) - u_{\alpha}(y_n,t)]^2}{k_B \sum_{i=1}^{N_{\text{fluid}}} H_n(y_i(t))} \ , \tag{12}$$

where α represents x, y, or z. At steady state, $u_y(y_n,t)$ and $u_z(y_n,t)$ are essentially zero for all n and so the values obtained for $T_y(y_n,t)$ and $T_z(y_n,t)$ are considered to be reliable estimates of the local temperature. However, $u_x(y_n,t)$ is a measure of the induced flow field and is of quite a substantial magnitude for the shear rates applied here. This causes a problem in the determination of local temperatures in the x direction as the use of $u_x(y_n,t)$ as the flow velocity for *all* positions within the nth slab can easily be shown to result in a systematic overestimation of $T_x(y_n,t)$ by a factor roughly proportional to Δy^2. To some extent, this error can be minimized by reducing Δy but unfortunately once the average number of particles per slab falls much below ~ 100, a significant underestimation takes over as there are no longer enough particles to give a reliable instantaneous estimate of the time-averaged slab flow velocity. As a compromise, we have used $N_{\text{slab}} = 40$, which gives a slab width $\Delta y \approx 1.4\sigma$.

The SB model has 37 500 fluid and 5610 boundary particles and the dimensions of the fluid system are L_x, 55.00σ; L_y, 48.54σ; and L_z, 16.52σ. The reduced density $\rho^* = N\sigma^3/V$ of the fluid is approximately 0.85 (the density cannot be specified exactly due to the uncertainty introduced by having a particulate wall structure). The separation of wall particles is σ in the x direction and $r_0 \cos(\pi/6)$ in the y and z directions, giving a reduced density of 1.06. The equations of motion are integrated

using the leap-frog form of the Verlet algorithm [19] using a time step of $\Delta t = 0.002\,26\tau$ where the usual Lennard-Jones time unit $\tau = (\varepsilon/m\sigma^2)^{-1/2}$. To check the stability of the algorithm at the very high temperatures generated under boundary driven shear (see later), equilibrium (NVE) simulations, using standard periodic-boundary conditions, were carried out with this time step at $T^* \sim 15$ and $\rho^* = 0.85$. No perceptible drift was seen in the total energy in $20\,000\Delta t$ and the root-mean-square deviations in the total energy were found to be acceptably low, $\sim 1\%$ of those in the potential energy.

In order to perform simulations using large-size systems more efficiently, a parallel molecular-dynamics (MD) algorithm for distributed-memory machines was developed. The algorithm is based on spatial decomposition and implemented on a Meiko computing surface [20]. The parallelized program shows good scaling properties and the efficiency is fairly constant over a wide range of system sizes.

C. Homogeneous-shear model

The (HS) method implemented is similar to that originally proposed by Lees and Edwards [2]. The system employed is periodic in all directions but the periodic images in the y direction are made to translate along the x axis in opposite directions. This sliding motion induces and maintains a shear flow within the fluid system. Apart from when $d\dot{\gamma}/dt$ is nonzero, this is equivalent to integrating the Sllod [8] equations of motion (so named because of their relationship to Dolls tensor algorithms), which although not derivable from a Hamiltonian do give an exact description of planar Couette flow as in their second-order form we are simply integrating Newton's equations in conjunction with the Lees-Edwards boundary conditions (see Ref. [8] for a detailed discussion of this and related points). As in the SB model, this shearing motion will result in a gradual increase in the temperature of the fluid system. However, in this case, to control temperature the momenta of all the fluid particles are rescaled at each time step using the *ad hoc* scheme. Our own unpublished data and those of others [9] have demonstrated that the various constant temperature algorithms produce essentially the same result for the viscosity. For a more detailed discussion of the connection between different thermostatting methods, the interested reader is referred to Ref. [9].

The system temperature was calculated from

$$T = \frac{1}{3N_{\text{fluid}}k_B} \sum_{i=1}^{N_{\text{fluid}}} m_i[\mathbf{v}_i - \mathbf{u}(\mathbf{r}_i)]^2 , \tag{13}$$

where we assume that the local flow velocity is simply given by

$$\mathbf{u}(\mathbf{r}_i) = (\dot{\gamma} y_i, 0, 0) . \tag{14}$$

Although this assumption has been shown to produce spurious results at very high shear rates [16], at the shear rates used in this study it is an acceptable assumption [17].

For the HS system, the various pressure tensors are calculated using the virial theorem as given by Eq. (7). Again, a linear velocity profile is assumed in order to estimate the streaming velocity required for the calculation of the kinetic contribution.

The system used for HS simulations contains 1000 particles and the potential parameters (ε and σ) used are the same as in the SB method. The density, temperature, and shear rate applied are determined from the SB simulations. In the HS simulations, the equations of motion are integrated using the leap-frog form of the Verlet algorithm [19] using a time step of $0.002\,26\tau$.

III. RESULTS

We used the SB model to study the shear viscosity at an applied shear rate of $0.4427\tau^{-1}$. A total of 340τ is required for the system to attain steady state and a further run of 113τ was performed to collect data for averaging.

The density profile across the system, $\rho^*(y_n)$, under steady-state shear is shown in Fig. 2. The ordering effect on the fluid due to the solid boundaries extends for a distance of about 4σ. This effect has been observed previously for both smooth [21] and structured boundaries [22–24]. Apart from this effect, the density profile in the middle region is smooth, as would be expected for a fluid. The profile is, however, not flat but shows a definite dip in the center, an effect which we shall show is related to the temperature profile through the system. To calculate the total volume occupied by the fluid, we summed the volumes of all the slabs which contained fluid particles. The mean fluid density at steady state using this definition is 0.848, which is slightly lower than the initial value. This occurs because the boundaries were pushed back as a result of the normal pressure generated in the fluid under shearing conditions (see Table I).

The temperature profile $T(y_n)$ is shown in Fig. 3. The function shown is actually the mean of the y and z temperatures since, as was explained above, the definition of the local temperature used here, Eq. (12), gives results for the x temperature which depend on the slab width. Differences between the y and z temperature profiles are very small, amounting to at most ~ 0.02 in reduced units,

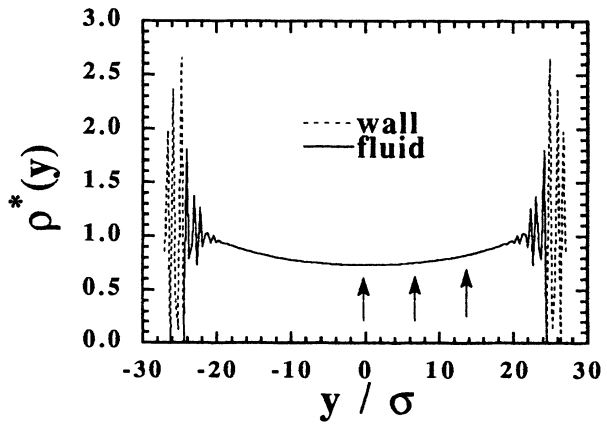

FIG. 2. The mean density profile at steady state for the SB model. The arrows indicate densities chosen for the homogeneous-shear simulations.

TABLE I. Pressure tensor calculated from the sliding-boundary simulation. The components P^*_{xx} and P^*_{zz} are calculated using the virial theorem, while the other two are calculated from the wall.

P^*_{xx}	P^*_{yy}	P^*_{zz}	$-P^*_{xy}$
36.28±0.02	36.28±0.02	36.25±0.02	1.01±0.01

which is of the same order as the statistical precision. The temperature profile is consistent with the trend observed in the density profile in that the region of lowest density, i.e., the center of the fluid regime, corresponds to that of highest temperature. Simple hydrodynamic theory [25] predicts a parabolic profile for a system sheared between walls at $y=\pm h$ held at a temperature of T_0:

$$T(y)=T_0+\frac{\eta\dot{\gamma}^2}{2\kappa}(h^2-y^2)\ , \tag{15}$$

but there are significant deviations from this form. The reasons for this discrepancy are that the theory assumes a constant thermal conductivity (κ) and a constant rate of energy production ($\propto\eta\dot{\gamma}^2$) between the walls. This is almost certainly incorrect since there are large variations in density, temperature, and, as will be shown, shear rate across the system. The continuous curve actually shown in Fig. 3 is a nonlinear regression least-squares fit of $T(y_n)$ to a fourth-order polynomial.

The x velocity (streaming) profile is found to be s shaped at the shear rate used (Fig. 4), and the average velocity of particles in the first layer of fluid (see Fig. 2) is within 2% of the wall velocity so that there is close to stick-boundary behavior. This result is consistent with a recent study by Thompson *et al.* [23]. We have fitted the velocity profile to a fifth-order polynomial:

$$u_x(y_n)=\sum_{k=0}^{5}C_k y^k\ , \tag{16}$$

using nonlinear least-squares regression. This is shown as the continuous curve in Fig. 4.

For the SB model, the viscosity is always calculated using the resultant stress on the boundaries $\langle -P_{xy}\rangle$. The

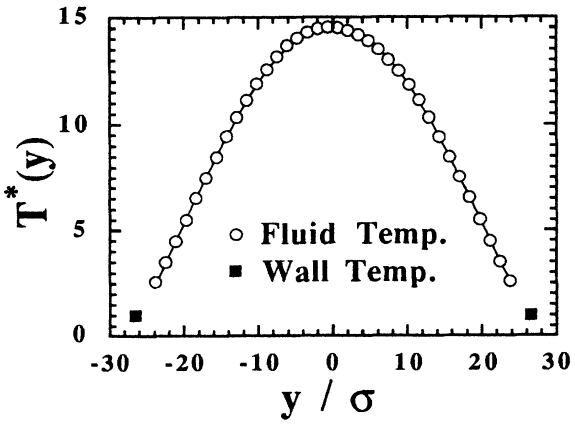

FIG. 3. The mean temperature profile at steady state for the SB model.

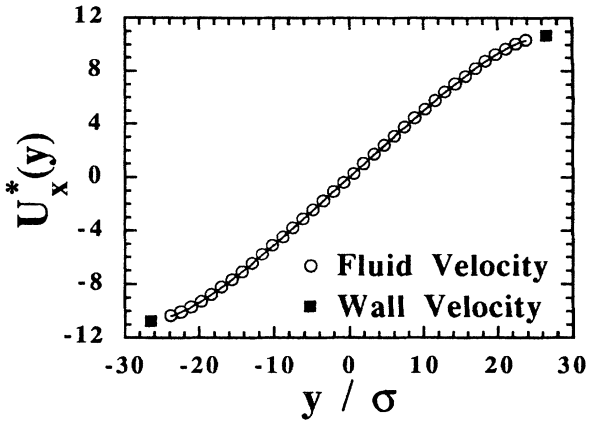

FIG. 4. The mean flow velocity in the x-direction profile at steady state for the SB model.

use of the average wall stress is justified in this calculation since for mechanical stability, the stress must be uniform across the system at steady state. This has also been verified numerically using direct calculations of both diagonal and off-diagonal components of the pressure tensor from the momentum flux across various planes parallel to the boundaries [26,27]. As discussed above, there are two problems associated with the calculation of the pressure tensor from the virial theorem in the system with explicit walls. In Table I average values are given for the components of the pressure tensor of interest here. P_{xx} and P_{zz} are calculated from the virial theorem and P_{yy} and P_{xy} are determined from the forces on the walls. The errors quoted are the standard errors determined using a method previously described [28]. Within these uncertainties, there are no significant differences in the normal components of the pressure tensor.

In the HS method the viscosity is calculated for an infinite homogeneous fluid at a well-defined state point. From the SB simulation we have calculated the "local" viscosities within the fluid, well away from the boundaries, from the induced local shear rate in the system at steady state. Numerically, the local induced shear rate $\dot{\gamma}(y)$ was obtained by differentiating the fitted streaming velocity profile, Eq. (16),

$$\dot{\gamma}(y)=\frac{du_x(y)}{dy}=\sum_{k=1}^{5}C_k k y^{k-1}\ . \tag{17}$$

From $\dot{\gamma}(y)$, the corresponding y-dependent viscosity $\eta(y)$ is given by

$$\eta(y)=\frac{\langle -P_{xy}\rangle}{\dot{\gamma}(y)}\ . \tag{18}$$

The results (Fig. 5) show that the induced shear rate increases gradually to a maximum from the boundary to the center of the system, which means the "local" viscosity decreases to a minimum at the center. This represents the local fluid viscosity, which can be used to compare with that calculated by the HS method.

An alternative way of calculating the viscosity at

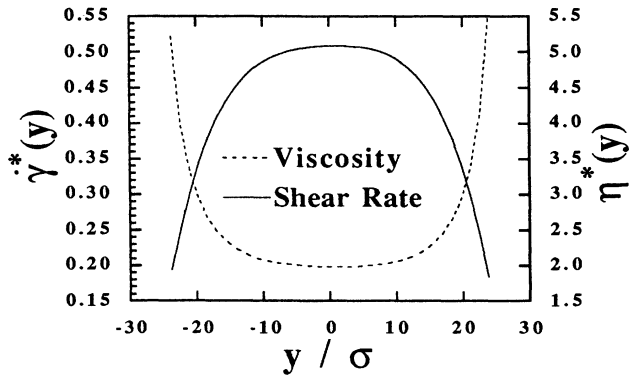

FIG. 5. The shear rate (left-hand scale) and viscosity (right-hand scale) profiles at steady state for the SB model.

steady state is to use the applied shear rate $\dot{\gamma}_a$ so that

$$\eta = \frac{\langle -P_{xy} \rangle}{\dot{\gamma}_a} . \tag{19}$$

The value so obtained is 2.28±0.02. This is the method that would be used in the laboratory. Although it has recently been experimentally demonstrated that viscosities are insensitive to the thickness of the liquid film down to distances of about ten molecular diameters [29], these experiments were performed at low shear rates where heating effects were not severe. For our model the large range of shear-induced temperatures and densities in the liquid makes it difficult to compare the viscosity calculated using Eq. (19) with HS results obtained at fixed density and temperature.

A. Comparisons between the two methods

To perform the comparison, HS simulations were carried out at three different state points corresponding to the steady-state temperatures, densities, and shear rates as found in the SB simulation at values of y equal to 0, 6.8σ, and 13.6σ. The exact conditions at each point are determined by substituting these values of y into the least-squares fits to the profiles $T^*(y)$, $\dot{\gamma}^*(y)$, and $\rho^*(y)$ obtained from the SB simulation (see Table II). These points are marked with arrows in the density profile (Fig. 2). The point at $y=13.6\sigma$ is close to that where the thermal gradient is a maximum but is far enough from the wall to be considered as being in the fluid regime. The $y=0$ point is at the center of the system where the thermal gradient is zero but the temperature is a maximum and the density is a minimum. The third point is intermediate between these two.

The HS systems at these three state points were allowed to evolve for about 100τ in order to reach steady state after which data were collected for averaging over the next 226τ. Values obtained for the significant components of the pressure tensor are shown in Table III along with other relevant data.

A comparison of the average pressure tensors obtained under SB and HS conditions can be drawn from Tables I and III. For the shear stress there is very good agreement within the statistical uncertainties. Consequently,

TABLE II. Results for the local viscosity and the particular conditions found at three locations in the sliding-boundary simulations. The density, temperature, and shear rate are determined from the various fitted profiles $T^*(y)$, $\dot{\gamma}^*(y)$, and $\rho^*(y)$. The viscosities are calculated using the induced shear rate and the average wall shear stress from Table I.

y/σ	$\dot{\gamma}^*(y)$	$T^*(y)$	$\rho^*(y)$	$\eta^*(y)$
13.603	0.4564	9.872	0.8271	2.21±0.02
6.802	0.4976	13.373	0.7556	2.00±0.02
0.000	0.5091	14.621	0.7342	1.95±0.02

the "local" viscosities from SB and HS simulations are also in good agreement (compare the final columns of Tables II and III). For the normal pressure components, if we compare the three HS simulations individually, there is good agreement among P_{xx}, P_{yy}, and P_{zz} for two of the three state points but for the lowest-density, highest-temperature point, P_{xx} is slightly higher. We do not consider this difference as being significant as it is only just larger than our estimated errors. Comparisons between the three HS simulations and the SB one show that there are some systematic deviations which we attribute to small errors in the original specification of the conditions (T^*, $\dot{\gamma}^*$, and ρ^*) under which the HS calculations were carried out. Again, these differences are not considered significant.

We conclude from this comparison that at a shear rate of about $0.4\tau^{-1}$, the HS method reproduces very well the pressure tensor measured using sliding boundaries at points in the fluid which span the range of temperatures (10 to $15\varepsilon/k_B$) and densities (0.73 to 0.82) for which conditions are at their most extreme.

The results obtained so far are in accordance with two recent studies aimed at investigating the effect of a thermostat in shear flow simulations. Loose [30] obtained excellent agreement for the shear viscosity of gases over a wide range of shear rates using kinetic theory and the HS method. Ciccotti *et al.* [21] used a stochastic wall system and found the viscosity is in agreement with those obtained from HS simulations for Lennard-Jones argon.

Unfortunately, it has not been possible to extend the SB simulations to shear rates where significant normal pressure differences and nonequipartition of the kinetic energy occur, $\dot{\gamma}^* \sim 2$, as the very high temperatures generated lead to fluid particles penetrating the wall. Attempts to "stiffen" the boundaries by using higher values of k_w proved counterproductive as this leads to a reduction in the rate of energy transfer between the fluid and the boundary particles and a consequent increase in the fluid temperature This decoupling behavior is well known for system with disparate characteristic frequencies [31]. Another possibility might be to modify the interaction potential between the wall and fluid particles in order to reduce penetration, but we have not explored this method.

In principle, we could reduce the high temperature of the system by shortening the distance between the walls. However, our system is only ~50 molecular diameters wide already and the walls have a detectable influence on

TABLE III. The results of homogeneous-shear simulations. The conditions used in the HS simulations (i.e., temperature, density, and shear rate) are determined from the various profiles $T^*(y)$, $\dot{\gamma}^*(y)$, and $\rho^*(y)$ obtained from sliding-boundary simulation.

$\dot{\gamma}^*$	T^*	ρ^*	P^*_{xx}	P^*_{yy}	P^*_{zz}	$-P^*_{xy}$	T^*_x	T^*_y	T^*_z	η^*
0.4564	9.872	0.8271	36.31±0.01	36.32±0.01	36.28±0.02	1.01±0.02	9.878±0.01	9.872±0.01	9.865±0.01	2.21±0.04
0.4976	13.373	0.7557	36.24±0.02	36.25±0.02	36.23±0.02	1.01±0.02	13.39±0.01	13.37±0.01	13.36±0.01	2.03±0.04
0.5091	14.621	0.7342	36.27±0.02	36.22±0.02	36.22±0.01	0.99±0.02	14.64±0.01	14.61±0.01	14.61±0.01	1.94±0.04

the density profile over 20% of this range, seriously reducing the volume of material which can be said to be shearing as a fluid. Ideally, we would like to simulate a much larger system where this immediate boundary effect is negligible and we can thus access the limiting bulk fluid behavior. Even assuming a quadratic dependence [Eq. (15)] of the maximum temperature on the distance between the walls means that if the temperature is not to increase, then a proportional reduction has to be made in the applied shear rate. This is a significant point, as in the laboratory the combination of the physical properties of the fluid and the material making up the boundaries, and the geometry of the system, must ultimately impose some upper limit to the temperature and hence strain rates that are accessible. In particular, the thermal conductivity plays an important role in determining the rate at which heat can be removed from the system. It is significant that even in our SB simulation, where the thermostatted walls provide a very efficient energy sink, enough heat is generated to cause severe problems in maintaining the integrity and functionality of the boundaries. Now, from the results presented here, we have seen that HS reproduces very well the pressure tensor at state points corresponding to local conditions appertaining to a boundary driven shear. It would seem from this that a fluid shearing with heat being removed at a *rate which is naturally realizable* either through conduction or homogeneously behaves in much the same way. What we cannot say is whether this will be the case when heat is removed at a rate far higher than physically possible, as can occur in HS simulations carried out at a fixed ("wall") temperature. It is perhaps significant, then, that for the atomic system being studied here, the phenomena of normal pressure differences and nonequipartition of kinetic energy manifest themselves in just such a regime.

IV. CONCLUSIONS

We have examined the validity of the HS method of studying shear flow by making comparisons with a SB method. The main difference between the two techniques is the way that heat energy is removed from the system. In the HS method the equations of motion are modified in order to extract kinetic energy in a homogeneous, though completely unphysical, manner. This is achieved more realistically in the SB method by conducting heat out through the boundaries. As a result, we observed the development of characteristic density, temperature, and velocity profiles between the boundaries. For the SB method adopted here, it transpired that the highest applied shear rate that could be studied was limited by the disruption caused to the boundaries by the viscous heat generated in the fluid. The results from an SB simulation carried out at an applied shear rate of $0.44\tau^{-1}$, close to this upper limit, were compared with those from HS calculations, using the local conditions at different points in the SB system as input. This comparison seems to indicate that the pressure tensor is largely insensitive to the method of removal of viscous heat provided that the rate at which it is dissipated is physically realizable.

Although the present results seem to provide some

validation for the HS method, we are unable to make comparisons in the more controversial region of shear rates in excess of $2\tau^{-1}$, where the phenomena of normal pressure differences and nonequipartition of the kinetic energy are manifested in HS simulations. At these very high shear rates, the amount of heat that has to be removed to maintain a fixed temperature in a HS simulation is far in excess of that which could ever be dissipated by thermal conduction. It seems unlikely that this artificial enhancement of the thermal conductivity has no effect on the rheological properties of a fluid, so we believe that the results of HS calculations must be treated with caution, especially when relating them to the properties of real shearing fluids.

ACKNOWLEDGMENTS

The authors wish to thank Shell Research (Thornton) for generously providing computing equipment, financial support, and the use of their facilities. Also, we would like to acknowledge their continuous help and encouragement throughout this work. Dr. Yanos Michopoulos is thanked for a critical reading of the original manuscript.

*Author to whom correspondence should be addressed.

[1] W. T. Ashurst and W. G. Hoover, Phys. Rev. A **11**, 658 (1975).
[2] A. W. Lees and S. F. Edwards, J. Phys. **5**, 1921 (1972).
[3] D. J. Evans and G. P. Morriss, Phys. Rev. A **30**, 1528 (1984).
[4] G. Ciccotti, G. Jacucci, and I. R. McDonald, J. Stat. Phys. **21**, 1 (1979).
[5] K. Singer, J. V. L. Singer, and D. Fincham, Mol. Phys. **40**, 515 (1980).
[6] W. G. Hoover, Annu. Rev. Phys. Chem. **34**, 103 (1983).
[7] D. Brown and J. H. R. Clarke, Phys. Rev. A **34**, 2093 (1986).
[8] D. J. Evans and G. P. Morriss, *Statistical Mechanics of Nonequilibrium Liquids* (Academic, London, 1990).
[9] D. J. Evans and B. L. Holian, J. Chem. Phys. **83**, 4069 (1985).
[10] S. Nosé, J. Chem. Phys. **81**, 511 (1984).
[11] W. G. Hoover, Phys. Rev. A **31**, 1695 (1985).
[12] D. J. Evans, W. G. Hoover, H. B. Failor, B. Moran, and A. J. C. Ladd, Phys. Rev. A **28**, 1016 (1983).
[13] D. J. Evans, G. P. Morriss, and L. M. Hood, Mol. Phys. **68**, 637 (1989).
[14] D. M. Heyes, J. Chem. Soc., Faraday Trans. **82**, 1365 (1986).
[15] R. Byron Bird, C. F. Curtiss, R. C. Armstrong, and O. Hassager, in *Dynamics of Polymeric Liquids,* 2nd ed. (Wiley, New York, 1987), Vol. 1, Chap. 3, pp. 99–166.
[16] D. M. Heyes, G. P. Morriss, and D. J. Evans, J. Chem. Phys. **83**, 4760 (1985).
[17] D. J. Evans and G. P. Morriss, Phys. Rev. Lett. **56**, 2172 (1986).
[18] *Molecular-Dynamics Simulations of Statistical-Mechanical Systems,* edited by G. Ciccotti and G. Hoover (North-Holland, Amsterdam, 1986), pp. 317–326.
[19] M. P. Allen and D. J. Tildesley, *Computer Simulation of Liquids* (Clarendon, Oxford, 1987).
[20] S. Y. Liem, D. Brown, and J. H. R. Clarke, Comput. Phys. Commun. **67**, 261 (1991).
[21] G. Ciccotti and C. Trozzi, Phys. Rev. A **29**, 916 (1984).
[22] S. Sharma and L. V. Woodcock, J. Chem. Soc., Faraday Trans. **87**, 2023 (1991).
[23] P. A. Thompson and M. O. Robbins, Phys. Rev. A **41**, 6830 (1990).
[24] J. Koplik, J. R. Banavar, and J. F. Willemsen, Phys. Fluid A **1**, 781 (1989).
[25] Shih-I Pai, *Viscous Flow Theory; 1 Luminar Flow* (Van Nostrand, Princeton, 1956), Chap. 4, pp. 48–53.
[26] J. A. Pryde, *The Liquid State,* edited by G. O Jones (Hutchison, London, 1966), pp. 146.
[27] D. H. Tsai, J. Chem. Phys. **70**, 1375 (1979).
[28] D. Fincham and D. Heyes, Adv. Chem. Phys. **63**, 493 (1985). See also Ref. [19].
[29] J. H. Cushman, Nature **347**, 227 (1990).
[30] W. Loose, Phys. Lett. A **128**, 39 (1988).
[31] J. L. Tuck and M. T. Menzel, Adv. Math. **9**, 399 (1972).